Tuning colloidal gels by shear

Soft Matter

Accepted Manuscript

ROYAL SOCIETY OF CHEMISTRY

www.rsc.org/softmatter

ARTICLE TYPE www. rsc.org/xxxxxx | XXXXXXXX

Tuning colloidal gels by shear

Nick Koumakis[a,b,c], Esmaeel Moghimi[a], Rut Besseling[c], Wilson C. K. Poon[c], John F. Brady[d] and George Petekidis[a]

Received Xth XXXXXXXXXX 20XX, Accepted Xth XXXXXXXXX 20XX
First published on the web Xth XXXXXXXXXX 200X
DOI: 10.1039/b000000x

Using a powerful combination of experiments and simulations we demonstrate how the microstructure and its time evolution is linked with the mechanical properties in a frustrated, out-of-equilibrium, particle gel under shear. An intermediate volume fraction colloid-polymer gel is used as a model system, allowing quantification of the interplay between interparticle attractions and shear forces. Rheometry, confocal microscopy and Brownian Dynamics reveal that high shear rates, fully breaking the structure, lead after shear cessation to more homogeneous and stronger gels, whereas preshear at low rates creates largely heterogeneous weaker gels with reduced elasticity. We find that in comparison, thermal quenching cannot produce the structural inhomogeneities created under shear. We argue that external shear has strong implications on the routes towards metastable equilibrium, and therefore the gelation scenarios. Moreover, these results have strong implications for material design and industrial applications, as mixing, processing and transport protocols couple to the properties of the final material.

1 Introduction

Improving material properties through intelligent design of their microstructure and molecular interactions is a central goal of material science that requires in-depth understanding of the fundamental physics involved. An additional control is provided by processing, i.e. the route followed in manufacturing or synthesizing a specific material, especially when out-of-equilibrium metastable states are involved. In mesoscopic soft matter systems, where building blocks self-assemble *en route* to thermodynamic equilibrium while affected by kinetic arrest[1], external fields are quite common[2] and increasingly utilized in experimental investigations[3–5]. Morover, as structural changes occurring during processing significantly influence the end product, external fields such as shear maybe utilized in smart applications of complex multicomponent materials ranging from flow of biological fluids[6], tissue engineering[7], food formulations[8] and personal care products[9] to drilling muds[10], ceramics[11] and high performance concrete [12].

Due to their large size and easily tunable interactions colloids are ideal for studying several open condensed matter physics problems such as the glass transition and the interplay between thermodynamic phases and metastable, non-ergodic states[13] which are ubiquitous in materials, industrial processes and biological systems. An additional parameter related the with glass transition and the jamming scenario is shear stress, which combined with temperature (or interparticle interactions) and volume fraction provides a generic unified jamming phase diagram[14]. Again colloids arise as a prominent model system where a wealth of structural and dynamical phenomena[15] such as shear induced melting (yielding)[16,17], slip[18,19], shear banding[20,21], ordering[22,23], shear induced jamming[24] and frozen-in stresses[25] can be studied.

At low concentrations of attractive or charge stabilized particles, shear and flow may cause cluster break-up[26–28], shear incuded aggregation leading to increased viscosity and elasticity[29–31] and delayed yielding[32] or collapse of the gel network[33,34]. On the other hand at high particle volume fractions and/or attraction strengths colloids at rest acquire a variety of solid-like, non-ergodic states due to the formation of a microscopic network structure[28,35–37]. If however high enough stresses (or strains) are applied, the network will break, often in multiple steps due to the existence of spatial heterogeneities [17,38–41] and flow in a strongly non-Newtonean manner, also exhibiting significant thixotropy and ageing[42,43]. Preshear may affect mechanical properties such as the yield stress and viscoelastic moduli[43,44], while depending on the shear rate, strong bond breaking or enhanced cluster formation is found in bulk[6,45–47], 2D[48], or microchannels[49]. The elucidation of such rich flow response can be brought about only through the study of model systems with tunable interactions and by deploying a combination of experimental techniques and sim-

† Electronic Supplementary Information (ESI) available: [details of any supplementary information available should be included here]. See DOI: 10.1039/b000000x/

[a] *FORTH/IESL and Department of Materials Science and Technology, University of Crete, 71110 Heraklion, Greece*
[b] *National Research Council of Italy-IPCF UOS Roma, 2, 00185, Rome, Italy*
[c] *School of Physics and Astronomy, University of Edinburgh, Mayfield Road, Edinburgh EH9 3JZ, United Kingdom*
[d] *Division of Chemistry and Chemical Engineering, California Institute of Technology, Pasadena, California 91125, USA*

ulations. This may provide detailed information to guide the formulation of a comprehensive theoretical framework with predictive power. One of the most commonly-used model systems for attractive particles is colloid-polymer mixtures where non-adsorbing polymer chains induce an attractive force between colloidal particles, with a strength and range that depend on the concentration and size of the polymer chains respectively[50,51].

In this paper we use a combination of rheology, rheo-confocal microscopy and computer simulations to demonstrate how the control of the externally imposed shear rate during rejuvenation (or processing), can tune the final structure and therefore mechanical properties of a model colloidal gel. Strong structural changes during flow as well as during gel reformation after flow cessation are corroborated by the interplay between shear and attractive forces. By computer simulation we find that structures created by shear may not be reproduced by instantaneous thermal quenching. Our findings have strong implications for material design and industrial processes, as they suggest how the implementation of well-defined modifications in mixing, processing and transport protocols of multicomponent systems can couple to, or alter the properties of final products.

2 Methods

For Rheo-confocal measurements, we used concentrated suspensions of sterically-stabilized poly(methyl methacrylate) (PMMA) nearly hard-sphere particles with radius $R = 830$ nm (determined by confocal imaging) suspended in a density and refractive index matching mixture of decalin and cyclobromoheptane. Depletion attractions were induced through the addition of non-adsorbing linear polystyrene (PS) chains with molecular weight $M_w = 7450000$ g/mol and a radius of gyration, $R_g = 113$ nm. We used samples with particle volume fraction $\phi = 0.44$, as determined by Voronoi volumes and particle tracking[52], and PS concentration, $c_p = 0.0022$ g/ml resulting in an interparticle attraction at contact of $U(2R) \simeq -16k_BT$ and a range of attraction $\xi \simeq 0.05$ according to[53]. Rheological experiments were used to measure flow curves (steady state stress versus shear rate) and linear viscoelastic moduli while confocal microscopy under shear provided simultaneous structural analysis. An Anton-Paar MCR501 rheometer with cone-plate geometry (50 mm and 0.01 rad angle) coupled with a fast scanning VT-eye confocal unit (Visitech) mounted on a inverted microscope (Nikon) was used. The bottom glass coverslip was roughened by sintering a mixture of sand granules (> 100 μm) and PMMA particles. Imaging was possible in the areas between the granules (≈ 1 mm) and measurements where taken in imaging volumes with linear flow profiles. 3D images were taken after shear cessation, and the evolution of void structures was examined. The

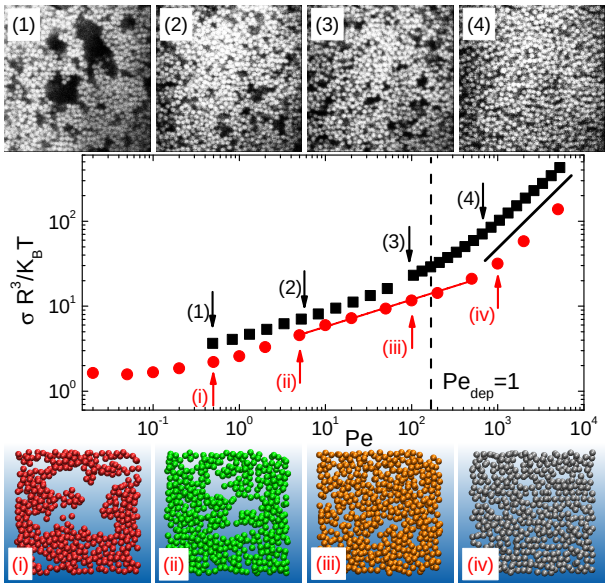

Fig. 1 Normalized stresses as a function Pe for BD simulations (red circles) and of Pe_{sc} for experiments (black squares), along with confocal (top) and simulation (bottom) images of structures under flow with rates indicated using arrows in the main figure. Experiments shown are at a volume fraction $\phi = 0.44$, potential depth at contact $U_{dep}(2R) \simeq -16k_BT$ and range of $\xi \simeq 0.05$ ($Pe/Pe_{dep} \simeq 160$). Simulations were set to $\phi = 0.44$, $U_{dep}(2R) = -20k_BT$ and $\xi = 0.1$ ($Pe/Pe_{dep} \simeq 100$). A power law slope of unity is shown for the higher rates (black line), while a power law fit discussed in the text is also shown.

shear rates in rheo-confocal experiments correspond to local values determined from flow profiles prior to shear cessation and have an estimated 10% standard deviation.

Rheo-confocal measurements were complemented by conventional rheometry using roughened cone-plate geometries that prevent slip. The long-time rheological response was studied using PMMA particles with $R = 400$ nm (determined by light scattering) and PS chains with $M_w = 283300$ g/mol and $R_g = 17$ nm, dispersed in decalin. The polymer concentration, $c_p = 0.0065$ g/ml at a particle volume fraction $\phi = 0.44$, gives and attractive potential of $U_{dep}(2R) \simeq -23.2k_BT$ and a range of attraction $\xi \simeq 0.03$[53].

For the cessation experiments, the samples were presheared starting from high shear rate (typically $100s^{-1}$), down to the shear rate in question, allowing for a steady state to be reached. As far as we have seen, both in experiments and simulations, the route followed to reach the final preshear rate after the high shear rate rejuvenation (i.e. directly or through a flow curve) did not affect the steady shear state reached during preshear.

In the case of the rheo-imaging, although the size of the cone truncation gap was of the order of the roughness, most of

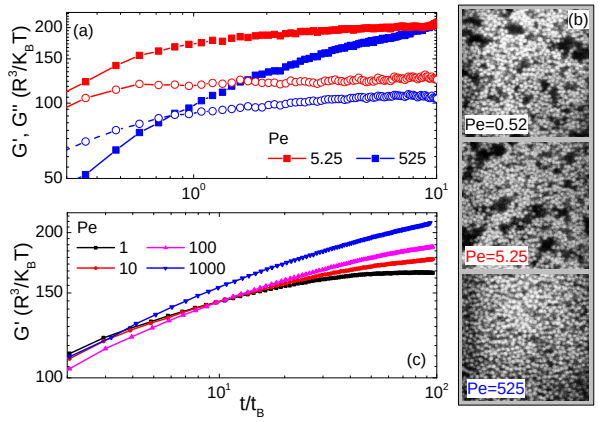

Fig. 2 a) Rheo-confocal experiments: Time evolution of the linear viscoelastic moduli of a colloidal gel at 1 rad/s ($R = 830$ nm, $\phi = 0.44$, $U_{dep}(2R) \simeq -16k_BT$, $\xi \simeq 0.05$, $Pe/Pe_{dep} \simeq 160$) after cessation of shear rejuvenation at high and low shear rates, as indicated: G' (solid symbols) and G'' (open symbols), b) Corresponding confocal images at $t = 10t_B$. c) Rheological measurements of a similar colloidal gel at 10 rad/s ($\phi = 0.44$, $U_{dep}(2R) \simeq -23.5k_BT$, $\xi \simeq 0.03$ and $Pe/Pe_{dep} \simeq 400$) with smaller spheres ($R = 400$ nm) allowing the determination of long time behavior (only G')

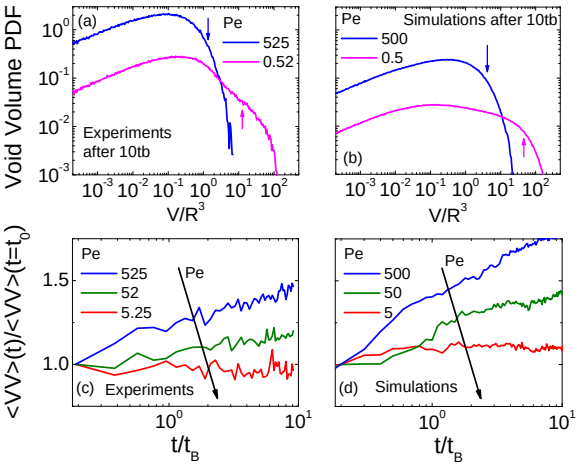

Fig. 3 Void volume probability density functions from experiments (a) and BD simulations (b) at steady state (at $10t_B$) after cessation of high and low shear rate flow as indicated. Time evolution of $\langle VV \rangle$, normalized by the initial state values (at $2t_B$), for high, low and intermediate rates from experiments (c) and BD simulations (d). Experiments are at $\phi = 0.44$, $U_{dep}(2R) \simeq -16k_BT$ and $\xi \simeq 0.05$ ($Pe/Pe_{dep} \simeq 160$). Simulations were set to $\phi = 0.44$, $U_{dep}(2R) = -20k_BT$ and $\xi = 0.1$ ($Pe/Pe_{dep} \simeq 100$).

the rheological torque arises from the outer part of geometry, where the actual gap is much larger. The corresponding confocal images were also taken towards the the edge of the cone. Moreover, conventional rheology measurements verified the findings.

We also performed Brownian Dynamics (BD) simulations that provide both mechanical information as well as detailed microstructure of the system under shear. Hard-sphere interactions were implemented through a potential-free algorithm [54] while attractions were included using an Asakura-Osawa (AO) potential[50] with similar parameters as our experiments. The range of attraction used was $\xi = 0.1$ with the attraction strengths, $U(2R) = -6$, -10, -20 and $-50k_BT$. This allows direct comparison between BD and experiments in terms of interactions, structure and stress response and examination of the validity of the Pe_{dep} scaling at various attraction strengths. In BD affine shear was applied on typically 5405 particles using periodic boundary conditions, while no crystallization was detected.

As BD simulations do not incorporate hydrodynamic interactions, there is a discrepancy with the short-time particle diffusion in a real experimental system. The latter is expected to be at least one order of magnitude smaller[55] in comparison with the free diffusion inside the highly concentrated clusters, in analogy with diffusion in a dense glass. Thus we scale the non-dimensional experimental Brownian time scale t_B, Pe (reflecting its scaled version, Pe_{sc}) and Pe_{dep} by an order of magnitude correction factor of 10 throughout the figures. Moreover, although the simulation parameters are chosen to be as close as possible to the experiments, we expect that experimental uncertainties in particle interactions (i.e. potential shape and depth) and volume fraction to produce differences when performing comparisons. Configurations were visualized with the open source Visual Molecular Dynamics (VMD) program[56].

3 Results and discussion

3.1 Steady state under shear

We study gels in which particles aggregate due to a "depletion" attraction induced by non-adsorbing polymer[50,51]. Experiments and BD simulations probe the microscopic structure of such depletion gels during steady shear as a function of shear rate as well as the linear viscoelastic properties during restructuring after cessation of shear. Experimentally, our depletion gels consist of PMMA hard-spheres and PS linear chains in suspension at $\phi = 0.44$ with an attraction strength well above the gelation threshold[37] while BD simulations[54] were conducted at similar Asakura-Oosawa (AO) interparticle potential[50] parameters. The steady state stress response of the gel at different shear rates, $\dot{\gamma}$, and typical slices of the microstructures are shown in figure 1 from rheo-confocal experiments and BD simulation data. Experiments and simula-

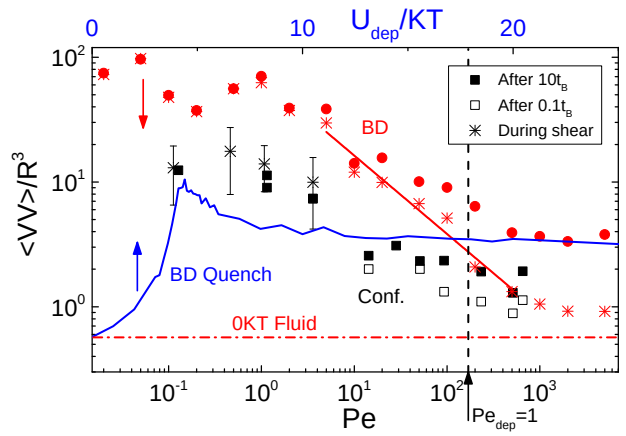

Fig. 4 Average void volume, $\langle VV \rangle$, from confocal microscopy (black) and BD simulation (red) at $\phi = 0.44$ under shear (stars, bottom axis) and after cessation (solid and open symbols, bottom axis) as a function of Pe. The blue solid line (top axis) represents $\langle VV \rangle$ from BD simulations (after $10t_B$) when quenching an equilibrium fluid at different attraction strengths. The value of $Pe_{dep} = 1$ is indicated with a vertical black line. The power law fit indicated by the sloid line is discussed in the text.

Figs 4, 5a	During shear	After 0.1t$_B$	After 10t$_B$	After Quench
Confocal	✳	□	■	
BD Sims	✳		●	—

Fig. 5 Quantities plotted in figures 4 and 5a.

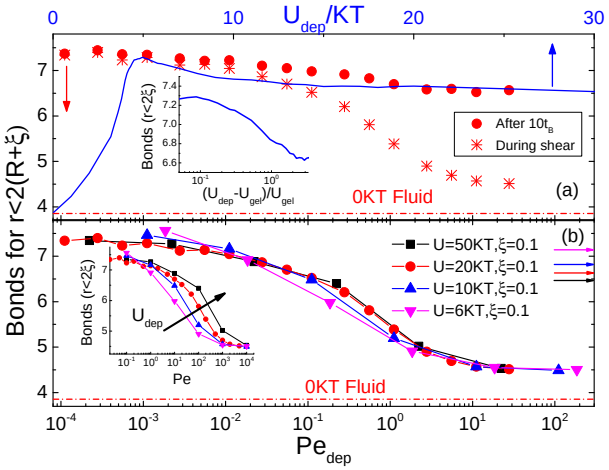

Fig. 6 a) Average number of bonds per particle (for $r < 2(R+\xi)$) as a function of Pe_{dep} from BD simulations ($\phi = 0.44$, $U_{dep} = -20k_BT$ and $\xi = 0.1$) during steady shear (stars, bottom axis) and after shear cessation (solid, bottom axis). The blue line (top axis) represents data from quenching an equilibrium fluid versus the attraction strength (after $10t_B$) and as a function of the distance from gelation (inset). b) BD data for sheared gels with $\phi = 0.44$ at different attraction strength as indicated versus Pe_{dep} calculated from eq. 1. Inset shows the same data as a function of Pe. Color coded horizontal arrows indicate the states produced from quenching an equilibrium fluid.

tions show strikingly similar flow curves and structures under shear, verifying that BD, although lacking of full hydrodynamic interactions (HI), captures efficiently the fundamental macromechanical and microstructural response of the system. Without attractions, the effect of shear can be quantified by the non-dimensional Peclet number, $Pe = \dot{\gamma} t_B = \frac{\dot{\gamma} R^2}{D}$, the product of the shear rate and the Brownian diffusion time, with the free diffusion coefficient, $D = D_0$ ($= \frac{k_B T}{6\pi\eta R}$, with R the radius of the particle and η the solvent viscosity) used in BD (in the absence of HI), while in experiments, the ϕ dependent short-time diffusion coefficient, $D(\phi)$, is used (the non-dimensional Peclet number is then denoted as Pe_{sc}).

Shearing at high Pe leads to a simple viscous stress response, where the stress increases linearly with shear rate, indicating that a strongly shear-melted colloidal gel flows as a Newtonian fluid. The corresponding snapshots of the structure under shear show that the gel network and clusters are broken down completely and the particles are distributed randomly as expected in the equivalent volume fraction fluid of hard spheres.

At lower Pe, the flow curve tends to a yield stress plateau typical of a soft matter solid[39,45]. Slightly above the yield stress the sample exhibits plastic flow with the stress increasing weakly with shear rate. Here both simulations and experiments reveal a shear thinning response with a sublinear power law increase of the stress with a power of about 0.32 for $5 \lesssim Pe \lesssim 500$. Microscopic imaging of the system in this regime reveals a highly inhomogeneous microstructure with large empty voids. Their size decreases with shear rate, suggesting that the shear thinning sublinear decrease of the apparent viscosity (equivalent to the stress increase) is due to a reduction of the cluster size with shear rate, in qualitative agreement with the behavior of lower volume fraction fractal clusters and gels[26,27].

When strong interparticle depletion forces are present, leading to clustering and gel formation, the $\dot{\gamma}$-dependent structural changes can be attributed to the balance between shear and depletion attraction. An estimate of this is given by a modified Peclet number, Pe_{dep}, which reflects the ratio of shear to depletion forces[38]

$$Pe_{dep} = \frac{F_{shear}}{F_{dep}} = \frac{6\pi\eta R(2\xi R)\dot{\gamma}}{U_{dep}(2R)/(2\xi R)} = \frac{12\pi\eta\xi R^3\dot{\gamma}}{U_{dep}(2R)} \quad (1)$$

with $U_{dep}(2R)$ the potential at contact and ξ the range of attraction. For $Pe_{dep} > 1$, bonds between particles are expected to get ruptured by shear forces and attractions do not affect

the structure, leading to liquid-like behavior. Conversely for $Pe_{dep} < 1$, the system is strongly affected by interparticle attractions, with shear enabling particles to explore configurational space and create compact clusters. Note that the ratio $Pe/Pe_{dep}(= U_{dep}(2R)/2k_BT\xi)$ depends only on the characteristics of the attraction potential and is independent of the shear rate.

3.2 Shear cessation

After cessation of shear (end of rejuvenation) the melted gel reforms, beginning from the steady-state structure created under shear. The linear viscoelastic properties evolve as shown in fig. 2a, where G' and G'' are plotted for low and high shear rates, along with corresponding confocal microscopy images (fig 2b) at $10t_B$ after shear cessation. An initial fast increase of both G' and G'' is followed by a slower evolution, indicative of further restructuring and gel coarsening. After a low shear rate preshear, the system almost instantaneously (for $t \lesssim 0.1t_B$) acquires a solid like response with $G' > G''$, and then evolves weakly with time until an almost steady state is reached after about $10t_B$. A preshear at high shear rates however, is followed by a stronger increase of G', starting from a liquid state but eventually creating a sample with stronger solid-like response, as evidenced by G' rising above the value following a weak shear rate rejuvenation.

Confocal images provide valuable information on the microstructural evolution of the gel. After a low shear rate preshear, the gel remains highly heterogeneous, essentially retaining the steady state structure acquired during shear (fig. 1). Higher shear rates show a continuous subtle evolution of the structure from a liquid-like to an interconnected network (see also supplementary confocal time-lapse movie). As inferred from the results shown in fig. 1, the *Pe* regimes where different behaviors arise are correlated to the power-law slopes of the flow curve (fig. 1). At high shear rates, where the stress increases linearly with shear rate, extended restructuring is expected after shear cessation as interparticle attractions become important again and the gel gets reformed. However, around the yield stress plateau, plastic flow takes place, particles are given ample time to reconfigure and compactify within clusters, while the system does not exhibit significant structural rearrangement after shear is stopped. Therefore by increasing *Pe* of preshear we observe a transition from a highly inhomogeneous gel created at low shear rates to a rather homogeneous network produced under high shear rates.

In fig. 2c we present additional rheological data on a similar colloid-polymer gel using smaller particles. In agreement with the rheological trends inferred from the rheo-confocal experiments, the elastic modulus exhibits a modest increase after weak preshear ($Pe_{dep} < 1$) in contrast with preshear at $Pe_{dep} > 1$, where stronger gel structures, with higher G', are created at long times. For longer waiting times and for both cases, the viscoelastic moduli were frequency independent (1-10 rad/s), while the transient, full frequency dependence was less accessible due to time constraints.

These additional measurements allow us also to monitor the rheological evolution at longer times. It should be noted that although samples for confocal imaging are close to density matched, using micron size particles introduces gravitational effects that precludes measurements longer than those presented here. At significantly longer times, G' and G'' may start decreasing, especially in the cases where dense clusters are formed, due to sedimentation.

We monitor structural heterogeneity using a real-space variable, as the structure factor for such intermediate volume fraction gels is less sensitive in revealing structural changes. Here we use the void volume, VV, which quantifies the volume of empty space (voids) in the gel[57]. VV of a point in space is defined as the volume of a sphere in contact with a particle surface, with the center of the sphere defining the position of the void in space. The probability density of the void volume, $VVPDF$, provides a quantitative measure of real-space heterogeneity (see supplementary figure). This analysis method was chosen over using a measure of the cluster size due to the ambiguity of defining the latter in a percolated gel.

In fig. 3 we plot the $VVPDF$ deduced from experiments and simulations after shear cessation and the time evolution of its average values, $\langle VV \rangle$. $VVPDF$ values smaller than the particle size ($VV < R^3$) represent gaps within close-packed areas, while higher values reflect large spatial heterogeneities (figs 3a and 3b). Confocal experiments and BD simulations show similar results: low shear rates produce highly heterogeneous systems, with large $VVPDF$ values, in contrast to high shear rates, as is visually evident in fig. 2b. By examining $\langle VV \rangle$ we may gauge the changes in heterogeneity with time, as shown in figs 3c and 3d, where lower shear rates are found to give rise to slower structural evolution than higher shear rates. Therefore, large structural heterogeneities are found to follow similar trends as the linear rheological properties of fig. 2a and 2c. In the shear-thinning regime, at intermediate shear rates, $5 \lesssim Pe \lesssim 500$, the void volume, or equivalently the average effective cluster volume, follows a power law decrease, $\langle VV \rangle \propto Pe^{-0.63\pm0.06}$, in agreement with the sublinear stress increase (power law slope ~ 0.32) measured rheologically in the same regime (see fig. 1).

3.3 Comparison to thermal quench

We now discuss the transition from the low to the high preshear regime, and further compare with the structure of a quiescent gel thermally quenched from an equilibrium liquid state. While the experimental system is not strictly tunable by temperature, simulations allow for thermal quenching by scaling

the interparticle potential. In fig. 4 we plot the *Pe* dependence of $\langle VV \rangle$ for the gel during and after cessation of shear, and contrast it with $\langle VV \rangle$ of the quiescent gel, determined at long times, as a function of attraction strength. Pe_{dep} defines the transition from the low to high shear rate regime. For $Pe_{dep} > 1$, homogeneous gels are formed after cessation of shear, very similar to those from a thermal quench, while the structure under shear approaches that of a simple liquid. On the other hand, for a preshear at $Pe_{dep} < 1$, larger voids are detected, and $\langle VV \rangle$ is found to be one or two orders of magnitudes higher than the liquid state value, defined by the average interparticle distance. The discrepancy in absolute values between experimental and simulation data seen in fig. 4 is mainly attributed to small differences in volume fractions, interactions and time scales (and thus *Pe*). However it should be noted that the absence of HI in BD may also influence the gel formation processes and structural details as seen previously in similar non-equilibrium states[58].

A comparison with instantaneously-quenched quiescent gels may provide insights into the mechanisms of restructuring under shear. Quiescent samples exhibit an increase of structural heterogeneity approaching the gelation point and a further decrease to a constant value at large attraction strengths well inside the gel regime[37]. At the same ϕ, the maximum heterogeneity in the quiescent gel is quite smaller than that produced by low rate preshear, although after $10t_B$ the system has not yet fully reached steady state.

We further examine the average number of bonds between particles, defined as the number of particle neighbors within the depletion attraction range[59]. Even though the information provided is limited to short distances, it identifies particle clustering and provides a complementary view of structural heterogeneity. Due to precision constraints we apply this type of analysis only to BD simulations data. In figure 6a the average number of bonds is plotted versus Pe_{dep} during and after cessation of shear. After a low shear rate preshear, the number of bonds remains largely constant with time, similar to the behavior of $\langle VV \rangle$. As high shear rate rejuvenation causes a complete disintegration of clusters, the number of bonds upon shear cessation increases with time as the gel reforms, although the absolute number of bonds remain smaller than after a low shear rate rejuvenation. In comparison, for the gel at rest, the number of bonds increases, reaching a maximum around gelation and subsequently drops to a constant at large attractions, similar to the behavior of $\langle VV \rangle$. Plotting the number of bonds as a function of the distance from the gelation point at $U_{dep}(2R) = -4.6k_BT$, we find a sigmoidal shape similar to the case under shear as a function of pre-shear rate (inset of fig. 6a).

Although the number of bonds follow a similar trend with the void volume, both quantifying spatial heterogeneity, the main difference of the former is that its maximum value after low shear-rate rejuvenation is similar to that of the quiescent sample at the gel point. This is due to the fact that the two quantities reflect the structure at different length scales; *VV* reflects an average over all length scales whereas the average bond number pertains to distances within the range of attraction. Therefore, for a given volume fraction and average bond number, a narrow distribution of bonds per particle is produced from a more homogeneous interconnected network with a smaller $\langle VV \rangle$, corresponding to the peak in thermal quenching at rest. In contrast, a rather broad distribution of bond numbers reflects inhomogeneous percolated clusters with larger $\langle VV \rangle$, as detected after low preshear rates. Therefore, comparing quenching near the gelation and preshearing at low rates, we find that although the average bonds are similar, the latter creates structures with larger voids and striking inhomogeneities.

Finally BD simulations with different depletion potentials provide further verification of the validity of Pe_{dep} scaling. As shown in fig. 6b, the number of bonds during shear for various attraction strengths fall onto a single master curve versus Pe_{dep}, even though in the quenched gel at rest the average bond number depends on the depth of potential.

4 Discussion

Our findings suggests that by tuning the way a colloidal gel is sheared or mixed, one may vary its final structure and mechanical strength without the need of changing the interparticle potential, and furthermore allowing access to structures that may not be accessible by thermal quenching, although during such manipulation one has to preclude the interference from other forces such as gravity. The ability of shear to change particle configurations at large length-scales implies that it may also affect the gelation scenarios[1,60], currently under intense investigation[59,61–63], as found for gels under the influence of gravity, which showed enhanced phase separation[64].

Applying strong shear (high Pe_{dep}) has an effect equivalent to an instantaneous thermal quench, promoting arrested phase separation, since upon shear cessation the system is a homogeneous fluid with strong attractive interactions present. On the other hand, weak shear (low Pe_{dep}), leads to lower free energy configurations corresponding to more compact clusters, akin of a low rate thermal quench that would produce similar densification through Brownian motion. Although Brownian motion alone cannot create such compact structures on a reasonable time-scale ($10t_B$), the microstructure created under weak shear may bring the system closer to thermodynamic equilibrium. Even if interacting systems with simple short range attractions are unlikely to produce quiescent equilibrium gels [1,59,61], we may expect that the application of shear can facilitate approach to such scenarios in other systems. A major difference in the final state accessed via thermal quenching

and shear should arise from the anisotropy associated with the latter, and the accompanied residual stresses. It is clear from previous work on creep and recovery[17] that after the application of shear, residual stresses remain, especially after low shear rates, as seen in hard sphere glasses[25]. This calls for a more extensive simulation study to compare thermal quenching with low shear rate shear-induced rejuvenation to unravel the underlying commonalities and differences. As a final note, in a reverse approach, one could infer the strength of interparticle interactions for a more complex attractive system by determining $Pe_{dep} = 1$, from either structural information under shear or by identifying the low to high shear rate viscosity transition through rheology.

5 Conclusions

The structural and rheological properties of intermediate volume fraction colloidal gels have been examined during steady-state shear flow and shear cessation using rheometry, confocal microscopy and Brownian Dynamics simulations. Through structural analysis of the steady state, we find that variation of the applied shear rate produces strong changes in the structure of the gels both during flow and gel reformation after flow cessation. Analysis of structural changes is carried out by determining the void distribution, a quantitative measure of spatial heterogeneity and the average number of interparticle bonds. At shear rates higher than Pe_{dep}, a non-dimensional shear rate representing the balance of shear and attractive interactions, particle networks and clusters break fully, whereas smaller rates produce large inhomogeneous structures due to compactification of clusters under shear. Such distinct microstructural starting states are the decisive factor for the evolution of the gel after shear cessation leading, at long times, to materials with different microstructures and mechanical properties. Gels reformed after strong shearing evolve into stronger solids with relatively homogeneous structure, whereas application of weak shear rates leads to gels with weaker elasticity and a highly heterogeneous microstructure.

We conclude that by tuning the way a colloidal gel is sheared or mixed, one may vary its final structure and mechanical strength, allowing access to structures with properties that may not be accessible by thermal quenching. By examining a well-defined model system, this work provides understanding on gelation scenarios subject to mechanical perturbations and has strong implications for general industrial applications where variations in mixing, processing and transportation protocols alter the final materials' properties, as well as for users that rejuvenate products by shaking. Such controlled microstructural manipulation may be used in manufacturing a diverse range of materials from controlled porosity and strength tissue scaffolds to high strength concrete formulations with desirable flow properties.

5.1 Acknowledgements:

We thank A. B. Schofield for particle synthesis. We acknowledge funding from EU FP7-Infrastructures "ESMI" (CP&CSA-2010-262348), Greek projects Thales "Covisco" and Aristeia II "MicroSoft" and UK EPSRC (grant EP/D071070/1).

#Current address: InProcess-LSP, Molenstraat 110, 5342 CC Oss, The Netherlands

References

1 E. Zaccarelli, *Journal of Physics: Condensed Matter*, 2007, **19**, 323101.
2 P. Vukusic and J. Sambles, *Nature*, 2003, **424**, 852–855.
3 K.-T. Wu, L. Feng, R. Sha, R. Dreyfus, A. Y. Grosberg, N. C. Seeman and P. M. Chaikin, *Proceedings of the National Academy of Sciences*, 2012, **109**, 18731–18736.
4 L. Di Michele, F. Varrato, J. Kotar, S. H. Nathan, G. Foffi and E. Eiser, *Nature Communications*, 2013, **4**, 2007.
5 S. Rose, A. Prevoteau, P. Elziere, D. Hourdet, A. Marcellan and L. Leibler, *Nature*, 2014, **505**, 382.
6 H. Chen, M. A. Fallah, V. Huck, J. I. Angerer, A. J. Reininger, S. W. Schneider, M. F. Schneider and A. Alexander-Katz, *Nature Communications*, 2013, **4**, 1333.
7 A. Zemel, I. B. Bischofs and S. A. Safran, *Physical Review Letters*, 2006, **97**, 128103.
8 R. Mezzenga, P. Schurtenberger, A. Burbidge and M. Michel, *Nature Materials*, 2005, **4**, 729–740.
9 C. Das, M. G. Noro and P. D. Olmsted, *Physical Review Letters*, 2013, **111**, 148101.
10 G. Maitland, *Current Opinion in Colloid and Interface Science*, 2000, **5**, 301–311.
11 H. Wyss, E. Tervoort and L. Gauckler, *Journal of the American Ceramic Society*, 2005, **88**, 2337–2348.
12 E. Masoero, E. Del Gado, R. J.-M. Pellenq, F.-J. Ulm and S. Yip, *Physical Review Letters*, 2012, **109**, 155503.
13 P. N. Pusey, *Liquids, Freezing and the Glass Transition*, Elsevier Science Publishers, North-Holland, Amsterdam, 1991, pp. 763–942.
14 A. Liu and S. Nagel, *Nature*, 1998, **396**, 21–22.
15 H. Lowen, *The European Physical Journal Special Topics*, 2013, **222**, 2727–2737.
16 T. G. Mason and D. A. Weitz, *Physical Review Letters*, 1995, **75**, 2770–2773.
17 K. N. Pham, G. Petekidis, D. Vlassopoulos, S. U. Egelhaaf, W. C. K. Poon and P. N. Pusey, *Journal of Rheology*, 2008, **52**, 649–676.
18 P. Ballesta, R. Besseling, L. Isa, G. Petekidis and W. C. K. Poon, *Physical Review Letters*, 2008, **101**, 258301.
19 J. R. Seth, L. Mohan, C. Locatelli-Champagne, M. Cloitre and R. T. Bonnecaze, *Nature Materials*, 2011, **10**, 838–843.
20 J. Dhont, M. Lettinga, Z. Dogic, T. Lenstra, H. Wang, S. Rathgeber, P. Carletto, L. Willner, H. Frielinghaus and P. Lindner, *Faraday Discussions*, 2003, **123**, 157–172.
21 R. Besseling, L. Isa, P. Ballesta, G. Petekidis, M. E. Cates and W. C. K. Poon, *Physical Review Letters*, 2010, **105**, 268301.
22 B. Ackerson and P. Pusey, *Physical Review Letters*, 1988, **61**, 1033.
23 N. Koumakis, A. B. Schofield and G. Petekidis, *Soft Matter*, 2008, **4**, 2008–2018.
24 D. Bi, J. Zhang, B. Chakraborty and R. P. Behringer, *Nature*, 2011, **480**, 355–358.
25 M. Ballauff, J. M. Brader, S. U. Egelhaaf, M. Fuchs, J. Horbach, N. Koumakis, M. Krüger, M. Laurati, K. J. Mutch, G. Petekidis,

M. Siebenbürger, T. Voigtmann and J. Zausch, *Physical Review Letters*, 2013, **110**, 215701.
26 R. Sonntag and W. B. Russel, *Journal of Colloid and Interface Science*, 1986, **113**, 399–413.
27 R. Wessel and R. Ball, *Physical Review A*, 1992, **46**, R3008.
28 J. Mewis and N. J. Wagner, *Colloidal Suspension Rheology*, Cambridge University Press, 2012.
29 J. Guery, E. Bertrand, C. Rouzeau, P. Levitz, D. A. Weitz and J. Bibette, *Physical Review Letters*, 2006, **96**, 198301.
30 C. O. Osuji, C. Kim and D. A. Weitz, *Physical Review E*, 2008, **77**, 060402.
31 A. Zaccone, D. Gentili, H. Wu, M. Morbidelli and E. Del Gado, *Physical Review Letters*, 2011, **106**, 138301.
32 S. B. Lindstrom, T. E. Kodger, J. Sprakel and D. A. Weitz, *Soft Matter*, 2012, **8**, 3657–3664.
33 S. W. Kamp and M. L. Kilfoil, *Soft Matter*, 2009, **5**, 2438–2447.
34 E. Secchi, S. Buzzaccaro and R. Piazza, *Soft Matter*, 2014, **10**, 5296–5310.
35 Y.-L. Chen and K. S. Schweizer, *The Journal of Chemical Physics*, 2004, **120**, 7212.
36 S. A. Shah, Y. L. Chen, K. S. Schweizer and C. F. Zukoski, *Journal of Chemical Physics*, 2003, **119**, 8747–8761.
37 M. Laurati, G. Petekidis, N. Koumakis, F. Cardinaux, A. B. Schofield, J. M. Brader, M. Fuchs and S. U. Egelhaaf, *Journal of Chemical Physics*, 2009, **130**, 134907.
38 N. Koumakis and G. Petekidis, *Soft Matter*, 2011, **7**, 2456–2470.
39 M. Laurati, S. U. Egelhaaf and G. Petekidis, *Journal of Rheology*, 2011, **55**, 673–706.
40 Z. Shao, A. S. Negi and C. O. Osuji, *Soft Matter*, 2013, **9**, 5492–5500.
41 J. Kim, D. Merger, M. Wilhelm and M. E. Helgeson, *Journal of Rheology*, 2014, **58**, 1359–1390.
42 D. Bonn and M. M. Denn, *Science*, 2009, **324**, 1401–1402.
43 G. Ovarlez, L. Tocquer, F. Bertrand and P. Coussot, *Soft Matter*, 2013, **9**, 5540–5549.
44 N. Y. Yao, C. P. Broedersz, M. Depken, D. J. Becker, M. R. Pollak, F. C. MacKintosh and D. A. Weitz, *Physical Review Letters*, 2013, **110**, 018103.
45 P. Ballesta, N. Koumakis, R. Besseling, W. C. K. Poon and G. Petekidis, *Soft Matter*, 2013, **9**, 3237–3245.
46 L. C. Hsiao, R. S. Newman, S. C. Glotzer and M. J. Solomon, *Proceedings of the National Academy of Sciences*, 2012, **109**, 16029–16034.
47 B. Rajaram and A. Mohraz, *Soft Matter*, 2012, **8**, 7699.
48 K. Masschaele, J. Fransaer and J. Vermant, *Journal of Rheology*, 2009, **53**, 1437–1460.
49 J. C. Conrad and J. A. Lewis, *Langmuir*, 2008, **24**, 7628–7634.
50 S. Asakura and F. Oosawa, *Journal of Chemical Physics*, 1954, **22**, 1255.
51 W. C. K. Poon, *Journal of Physics: Condensed Matter*, 2002, **14**, R859.
52 R. Besseling, L. Isa, E. R. Weeks and W. C. Poon, *Advances in Colloid and Interface Science*, 2009, **146**, 1 – 17.
53 G. J. Fleer and R. Tuinier, *Physical Review E*, 2007, **76**, 041802.
54 D. R. Foss and J. F. Brady, *Journal of Rheology*, 2000, **44**, 629–651.
55 A. Sierou and J. F. Brady, *Journal of Fluid Mechanics*, 2001, **448**, 115–146.
56 W. Humphrey, A. Dalke and K. Schulten, *Journal of Molecular Graphics*, 1996, **14**, 33–38.
57 M. D. Haw, *Soft Matter*, 2006, **2**, 950–956.
58 A. Furukawa and H. Tanaka, *Physical Review Letters*, 2010, **104**, 245702.
59 J. C. F. Toledano, F. Sciortino and E. Zaccarelli, *Soft Matter*, 2009, **5**, 2390–2398.
60 W. C. K. Poon and M. Haw, *Advances in Colloid and Interface Science*, 1997, **73**, 71–126.
61 P. J. Lu, E. Zaccarelli, F. Ciulla, A. B. Schofield, F. Sciortino and D. A. Weitz, *Nature*, 2008, **453**, 499–503.
62 E. Zaccarelli and W. C. K. Poon, *Proceedings of the National Academy of Sciences*, 2009, **106**, 15203–15208.
63 A. P. R. Eberle, N. J. Wagner and R. Castaneda-Priego, *Physical Review Letters*, 2011, **106**, 105704.
64 J. M. Kim, J. Fang, A. P. R. Eberle, R. Castañeda Priego and N. J. Wagner, *Physical Review Letters*, 2013, **110**, 208302.